3 Results

3.1 Architecture of the Non-Translating 80S Ribosome

The large ribosomal subunit interacts with a number of proteins and protein complexes involved in cotranslational protein transport across the ER (reviewed in Johnson and van Waes, 1999; Schnell and Hebert, 2003). The oligo-saccharyl-transferase (OST) had initially been identified as “ribophorin” and like the oligomeric assembly of the trimeric Sec61p complex, it is one of the ribosome receptors in the ER membrane in higher eukaryotes (Marcantonio et al., 1984; Yu et al., 1990). The SRP-SR targeting system interacts with the ribosome to target the RNC complex to the ER membrane.

A three dimensional reconstruction of the non-translating 80S ribosome from *S. cerevisiae* in complex with the detergent solubilized trimeric Sec61p complex showed a single attachment point between the Sec61p complex and the large 60S subunit (Beckmann et al., 1997). Interestingly, the aqueous pore formed by the Sec61p complex aligned perfectly with the opening of the tunnel in the large ribosomal subunit that had been suspected to be the exit point for nascent chains in the 60S subunit. Based on biochemical evidence, the area surrounding this exit tunnel, was believed to be the main interaction site for the interaction of the ribosome with the ER membrane. The affinity of the ribosome to the ER membrane has to be tightly controlled. Only ribosomes with nascent chains bearing signal sequences should be targeted to the ER. The SRP mediated targeting pathway increases the affinity of the RNC for its ER receptors by several magnitudes. Thus, any structural changes that could regulate the affinity of the ribosome for its ER membrane receptors should be observed around the tunnel exit site at the large ribosomal subunit.

To test whether structural changes of the eukaryotic ribosome are involved in the regulation of its affinity for the ER membrane, we calculated a three dimensional electron

density map using cryo-EM and single particle imaging of a non-translating 80S ribosome from yeast in order to compare the structure to known structures of the 80S ribosome engaged with components of the translocation and targeting machinery.

3.1.1 Purification of Non-Translating Ribosomes

Ribosomes from yeast strain *Egd2aprA* were prepared essentially as described (Beckmann et al., 1997) using subcellular fractionation methods resulting in a fraction of ribosomes running as a single 80S peak on a 10-30% sucrose gradient. An aliquot of the gradient peak fraction showed a typical ribosomal protein pattern when stained with coomassie blue (Figure 3.2). The optical density (OD) at 280 nm of the ribosomal fraction was determined to be 415 OD/ml.

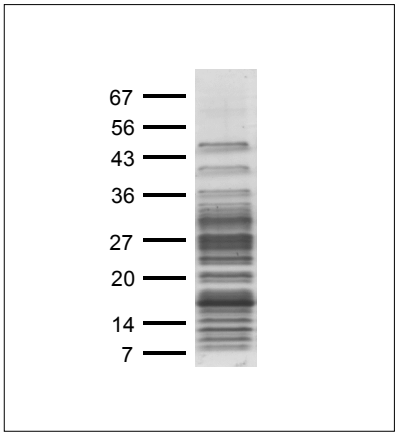

Figure 3.1: Ribosome Purification. Denaturing SDS page gel electrophoresis of 0.25 OD of purified non-translating 80S ribosomes on a 4-20% gradient gel, stained with Coomassie Blue. Molecular weights are indicated in kDa.

3.1.2 Preparation of Cryo Electron Microscopy Grids of Non-Translating Ribosomes

The purified non-translating ribosomes were used to prepare cryo-EM grids for image reconstruction. The non-translating ribosomes were diluted with ribosome dilution buffer to an OD_{280}=3.0/ml, and the diluted sample was used to prepare cryo EM grids. The grids were stored under liquid nitrogen.

3.1.3 Image Reconstruction of Non-Translating Ribosomes

The grids of non-translating ribosomes were used for structure determination by cryo-EM and single particle imaging. Micrographs were recorded in a defocus range of 0.8 µm to 2.4 µm on a Phillips CM 12 and scanned using a HiScan drum scanner (Eurocore, Saint-Denis, France) with a pixel size of 4.78 µm on the optical scale.

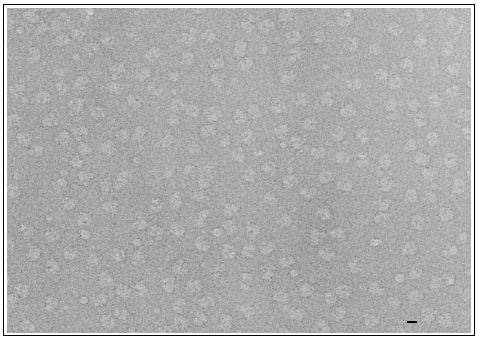

Figure 3.2: Cryo electron micrograph showing a field of vitrified non-translating 80S ribosomes.. Scale bar showing 200 Å.

The quality of each micrograph was checked by optical diffraction and micrographs showing obvious signs of either drift or astigmatism were discarded.

3.1.3.1 Multireference Alignment

An existing 3D volume of the 80S ribosome in complex with the Sec61p complex (Beckmann et al., 1997) was used to create a set of 83 reference projections, the electron density of the Sec61p complex was masked and 83 reference projections (views of the ribosome at known angles) were created using angular steps of 15 degrees (Figure 3.3) .

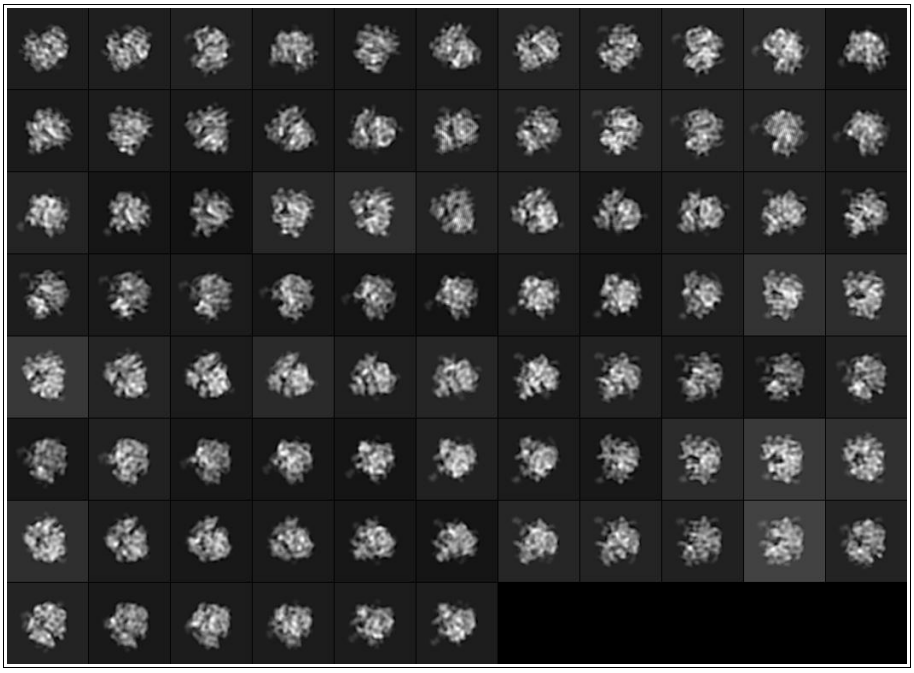

Figure 3.3: Reference projections. 83 Reference projections were obtained from an 80S ribosome using angular steps of 15 degrees.

A single raw image per particle was obtained by an automated particle searching procedure and manually inspected for quality. All selected raw images were aligned with the reference projections resulting in translational and rotational parameters as well as a

cross-correlation coefficient for the best matching projection for each raw image. The determined parameters were used to align all raw images. All images were segregated into 17 defocus groups based on the defocus each micrograph was recorded at. The rotational 1D power spectra of the micrographs in each defocus group were plotted to ensure they were in phase (Figure 3.4).

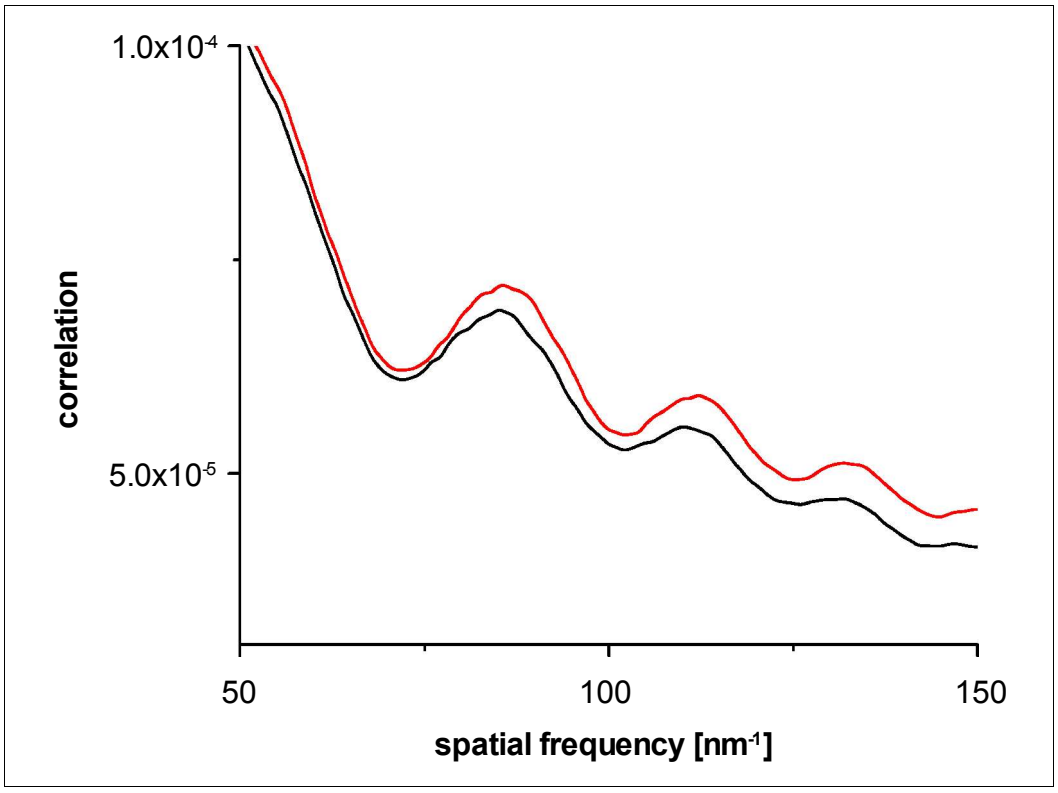

Figure 3.4: Power spectra plots. The 1D rotational power spectra of micrographs in each defocus group were examined to ensure they were in phase (shown are the power spectra of micrographs 17 (red line) and 19 (black line)).

Some of the 83 angular directions (images that were assigned to match one of the 83 reference projections) were over represented and the number of images per direction

was therefore limited to 60 images. Images of higher quality were selected by removing images with a cross-correlation coefficient lower than 1000.

3.1.3.2 Calculation of an Initial 3D-Model

After the selection process, 14.028 images (~75% of the original raw images) were selected to calculate an initial 3D density map. The resolution of the initial structure of the non-translating 80S ribosome was based on the Fourier shell correlation criterion using a cut off at 0.5 and determined to be 34 Å (Figure 3.5).

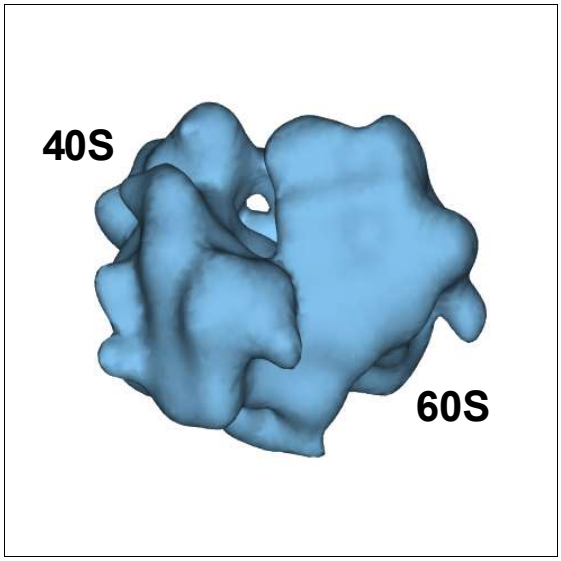

Figure 3.5: Cryo-EM structure of the initial 3D electron density map of the non-translating 80S ribosome. The resolution of the initial structure was based on the Fourier shell correlation criterion using a cut off at 0.5 and determined to be 34 Å.

3.1.3.3 Iterative Refinement of the Initial 3D-Model

The quality of the initial alignment was limited by the coarse angular steps chosen to create projections from the reference particle. In the final iterative refinement procedure, the selected raw images were reprocessed to increase the resolution of the structure. During the refinement procedure, the angular step size was reduced from 15 degrees to smaller values which led to an increased number of angular directions and thus to a higher number of reference projections (Table 3.1). Hence, each raw image was compared to a higher number of existing projections covering the reference structure of the reference allowing the determination of translational and rotational parameters as well as matching projections at higher resolution.

angular step size [°]	*number of angular directions*
15.0	83
2.0	5088
1.5	9076

Table 3.1: Number of angular directions in dependency of the angular step size.

The refinement of the initial 3D structure of the non-translating 80S ribosome included six iterative rounds of refinement for each defocus group. The angular step size used in the in the first five rounds of refinement was 2.0 degrees. The final round of refinement used an angular step size of 1.5 degrees. A combined 3D electron density map was calculated in every round of the procedure to judge the quality of the refinement procedure (data not shown).

Figure 3.6 shows the final structure of the non-translating 80S ribosome determined at 24.8 Å based on the Fourier shell correlation criterion using a cut off at 0.5.

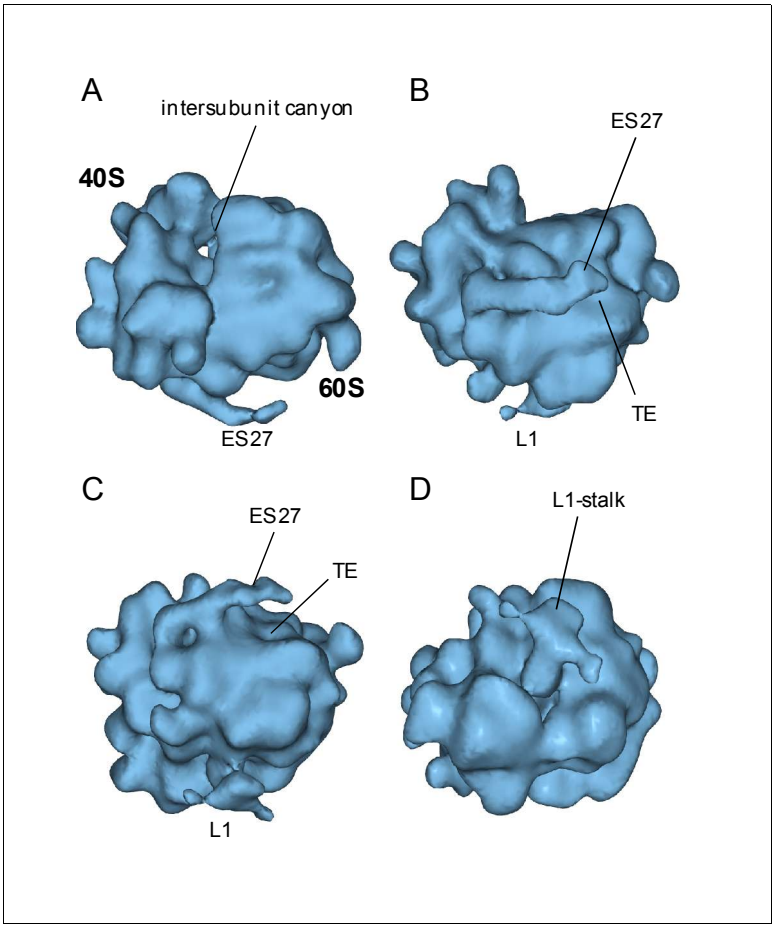

Figure 3.6: Cryo-EM structures of the non-translating 80S ribosome from yeast. **(A)** Same view as in figure 3.5, showing the 80S ribosome with its subunits clearly distinguishable, 40S on the left and 60S on the right. Note the extra mass originating at the bottom of the large ribosomal subunit (ES27). **(B)** Same as in (A) but rotated 90º so that ES27 is in front of the ribosome. Note that ES27 is blocking the tunnel exit of the large ribosomal subunit (TE). **(C)** Same as in (B) but rotated another 45º. Note that the tip of ES27 is covering the tunnel exit (TE). **(D)** Same as in (C) but rotated another 45º.

The calculated 3D structure had the typical overall appearance of an 80S ribosome. The 40S and 60S subunits were clearly distinguishable showing the empty inter-subunit canyon between the two ribosomal subunits (Figure 3.6, panel A). Interestingly the L7/L12-stalk, one of the landmarks of the large ribosomal subunit, was not visible in the structure, indicating structural changes in the 60S subunit dependent on the functional state of the ribosome. The electron density at the exit site of the inter-subunit canyon could be attributed to the L1-stalk of the 60S subunit. It was visible in the “closed” and the “open” conformation, indicating that the ribosomal fraction contained a mixed population of the two forms (Figure 3.6, panel D).

3.1.4 Movement of Expansion Segment 27

Close to the known attachment site of the protein conduction channel (Beckmann et al., 1997), the large ribosomal subunit beared a rod-like density 150 Å in length with a twist typical for helical rRNA (Figure 3.6, panel A, B and C). It originated at the subunit interface and was identified as the main helix of expansion segment 27 (ES27) of the 25S rRNA, one of the rRNA insertions characteristic for 80S ribosomes (Gerbi 1996), for details, see (Spahn et al., 2001). In several reconstructions of different yeast ribosome complexes (Beckmann et al., 1997; Gomez-Lorenzo et al., 2000; Morgan et al., 2000; and Helmers, unpublished), this helix can be found close to the L1 arm (L1 position) but also, following a counterclockwise rotation by 90º, reaching over the tunnel exit site (exit position) (Figure 3.6, panel B and C). The preference for one or the other position varies in these reconstructions, and often density is present in both positions.

We suggest, therefore, that the ES27 helix is a highly dynamic structure with two main conformations in a functional equilibrium (Figure 3.7). Notably, in reconstructions of ribosome-channel complexes, the ES27 helix was located exclusively in the L1 position, thereby not interfering with the channel in the exit position (Figure 3.7). Thus, binding of

the channel to the ribosome must coincide with a conformational change in the ribosomal periphery, shifting the equilibrium for the ES27 helix entirely to the L1 position.

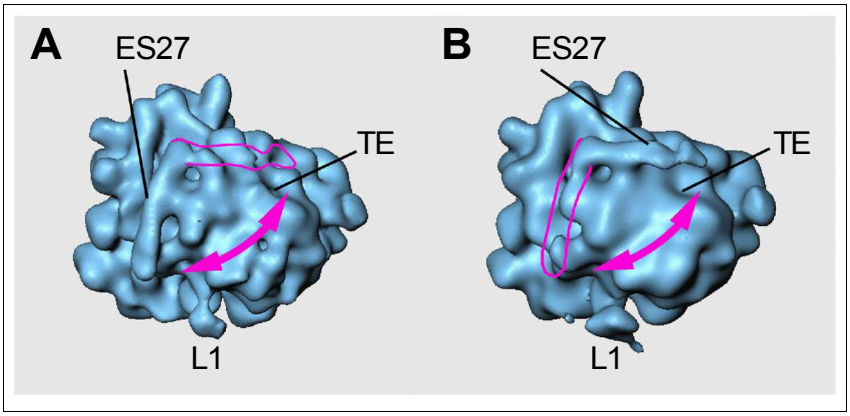

Figure 3.7: Dynamic expansion segment 27 (ES27). **(A)** The reconstruction of a ribosome-Sec61 complex in Triton X-100 (Beckmann et al., 1997) shown without the channel density. TE marks the tunnel exit and L1 the L1 protrusion. Note the expansion segment 27 (ES27) in the L1 position, distant from the tunnel exit. The pink contour shows the exit position of ES27 as observed in (B).
(B) A reconstruction of the ribosome without attached Sec61 complex at a resolution of 24.8 Å. Note that in this structure no density is visible in the L1 position. Instead, the ES27 is in the exit position with its tip in close proximity to the tunnel exit. The pink contour shows the L1 position as observed in (A).

3.2 Architecture of the Protein-Conducting Channel in Association with the Translating 80S Ribosome

The first cryo-EM structure of the Sec61p complex in association with the 80S ribosome (Beckmann et al., 1997) showed the Sec61p complex positioned such that the central pore aligned with the exit tunnel of the large ribosomal subunit representing the conduit for the nascent chain. However, it was not clear on what structural basis the ribosome-PCC complex is able to maintain the ion permeability barrier in its different modes of function during cotranslational protein transport, since the structure showed a gap of 15Å between the ribosome and the Sec61p complex.

3.2.1 Purification of Ribosome Nascent Chain Complexes

We chose a strategy to first isolate a homogeneous population of ribosome-nascent chain complexes (RNCs) carrying a signal sequence and then, in a second step, to use these RNCs for reconstitution of the RNC-channel complex in a membrane-free system for cryo-electron microscopy and 3D reconstruction. As a nascent chain, we used the first 120 amino acids of the yeast vacuolar type II membrane protein dipeptidyl-amino-peptidase B (DAP2), which is translocated cotranslationally *in vivo* (Ng et al., 1996). The transmembrane domain of this protein in position 30 to 45 serves as an uncleaved signal sequence, which inserts into the membrane in a loop resulting in a cytosolic orientation of the N-terminus.

The ribosomes were programmed in a yeast cell-free translation system with a truncated synthetic mRNA lacking a stop-codon. Under optimized conditions, this led to 15–20% stalled ribosome-nascent chain complexes with the nascent chains still bound to tRNA in the P site of the ribosome. In order to immuno-purify RNCs on the basis of the presence of the nascent chain, we translated mRNA encoding for the 120 N-terminal residues with an additional N-terminal HA-tag (9 amino acids). Translation of the truncated mRNA of

both the tagged and the untagged construct (called HA-DP120 and DP120) resulted in the appearance of two major bands on the autoradiography after SDS-PAGE (Figure 3.8).

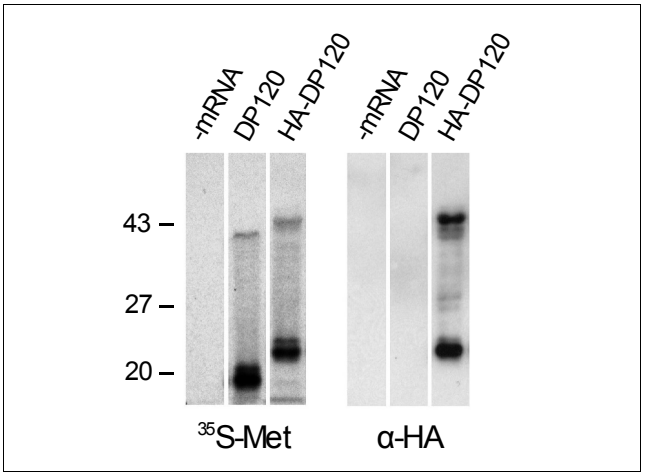

Figure 3.8: Truncated mRNA coding for the first 120 amino acids of dipetidyl-amino-peptidase B with (HA-DP120) or without (DP120) N-terminal HA-tag was translated in a yeast cell free system in the presence of ^{35}S-labeled methionine. The translation reaction was subjected to SDS-PAGE, blotted onto nitrocellulose, and either autoradiographed (left) or probed using a monoclonal anti-HA antibody (right).

The lower band represented the translated polypeptide while the larger product migrating at about 40 kDa represented polypeptide still bound to tRNA (peptidyl-tRNA). A smear reaching from the higher to the lower band is a result of ongoing hydrolysis of the peptidyl-tRNA bond in the basic environment of the gel during the run (Figure 3.8). Treatment with puromycin after translation led to a single band below 25 kDa and disappearance of the smear (data not shown). The translation products of the HA-tagged construct ran slightly higher than the untagged ones and were recognized by a monospecific antibody (Figure 3.8, right).

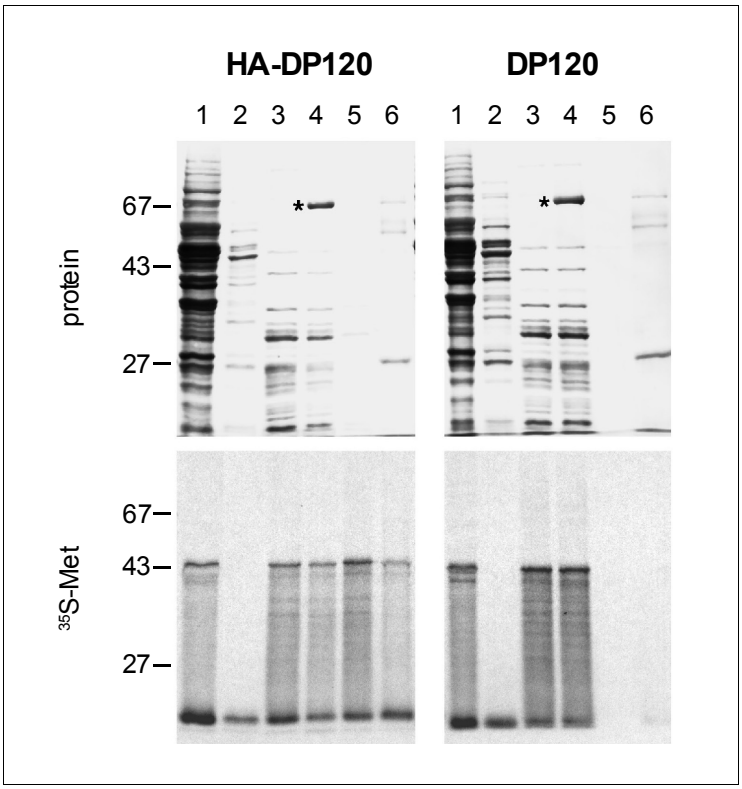

Figure 3.9: Translation reactions with tagged and untagged nascent chains were subjected to an analytical immunopurification procedure. Aliquots of fractions were applied to SDS-PAGE, blotted onto nitrocellulose, amido black stained (Protein), and autoradiographed to detect nascent polypeptide chains (^{35}S-Met); lane 1: total, lane 2: supernatant, lane 3: crude ribosomes, lane 4: depleted crude ribosomes after antibody and magnetic bead incubation, lane 5: eluate using excess HA-peptide, lane 6: magnetic beads after elution. Note the enrichment of HA-DP120 RNCs (lane 5) and the background-free control eluate (lane 5 for DP120). Asterisks mark bovine serum albumin, which is part of the antibody preparation.

A crude ribosome fraction was isolated by spinning the translation reaction through a high salt/high sucrose cushion, which also resulted in dissociation of non-ribosomal proteins from RNCs. The mixture of empty ribosomes and RNCs was then incubated with

a biotinylated anti-HA antibody and streptavidin-coupled magnetic beads. After washing the beads with high salt and detergent containing buffers, the bound RNCs were eluted by incubation with an excess of HA-peptide and spun through a sucrose cushion again. For the tagged construct, this procedure resulted in a highly enriched RNC fraction (Figure 3.9) with small amounts of ribosomal proteins detectable, but a strong ^{35}S-signal due to the presence of labeled nascent chains.

However, the same purification procedure did not lead to any detectable background when performed with the untagged control construct (DP120) (Figure 3.9). We scaled the procedure up in order to purify sufficiently large amounts (0.25 OD_{260}, 10 pmol) for further studies. The isolated RNCs showed the typical pattern of ribosomal proteins (Figure 3.10) and were stable for at least 9 hours on ice without significant hydrolysis or dissociation of the peptidyl-tRNA (data not shown).

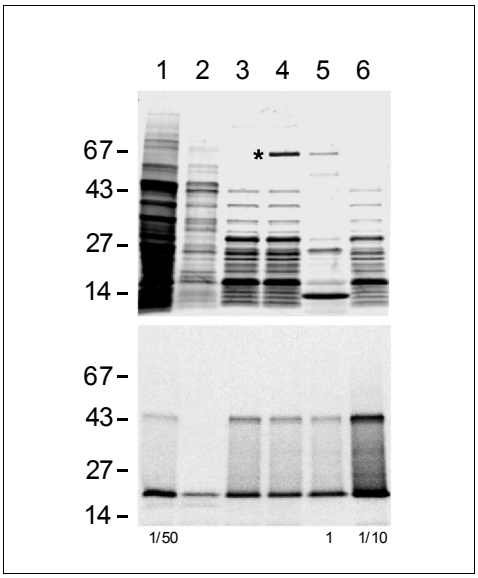

Figure 3.10: Same as shown for HA-DP120 in (Figure 3.9) but scaled up for preparative purpose. Note the characteristic pattern of ribosomal proteins in the peptide eluate (lane 6).

Thus, we describe the first method for the isolation of a homogeneous fraction of programmed (80S) ribosomes that (i) carry a chosen nascent chain kept in place by the P-site tRNA, (ii) are virtually free of empty ribosomes and additional factors, (iii) are stable enough for further experiments, and (iv) can be isolated in quantities sufficient for biochemical or structural studies.

3.2.2 Reconstitution of the Sec61p–Ribosome Nascent Chain Complex

Next, we attempted to reconstitute the active, i.e. translating and translocating, ribosome-channel complex using the RNC preparation and purified Sec61 complex (Beckmann et al., 1997) in a membrane-free system. The length of the nascent chain (HA-DP120) was chosen such that the signal sequence and at least 40 additional amino acids between the signal sequence and the C-terminus should be fully emerged from the tunnel of the large ribosomal subunit (Blobel and Sabatini, 1970). This spatial situation is known to facilitate a productive interaction of the signal sequence with the channel leading to the insertion of the nascent chain as a loop (Shaw et al., 1988; Jungnickel et al., 1995 and Mothes et al., 1998). The RNCs were incubated with increasing amounts of solubilized Sec61 complex under different conditions, and nascent chain insertion was monitored by protease protection assays. After digestion of RNCs alone with proteinase K, the nascent chain signal shifted completely to a lower molecular weight (regardless of the presence or absence of lipids), demonstrating that only a small part, which is buried in the ribosomal tunnel (30-35 amino acids), was protected (Figure 3.11).

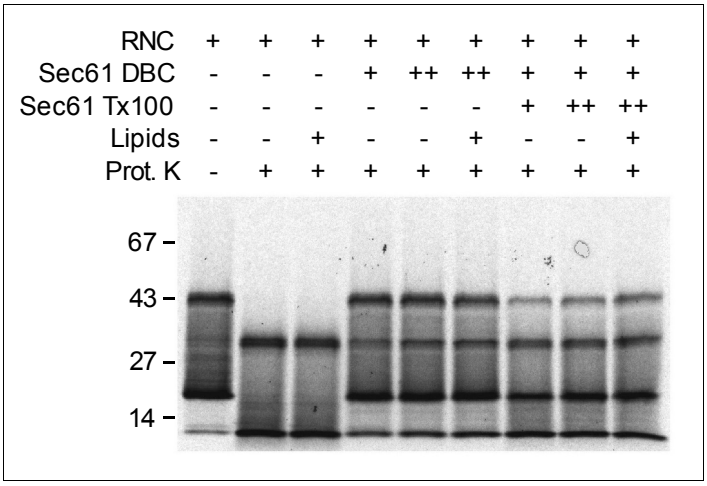

Figure 3.11: Immunpurified RNCs carrying the HA-DP120 chain were reconstituted with different amounts of solubilized Sec61 complex in DeoxyBigCHAP (DBC) or Triton X-100 detergent in the presence or absence of phospholipids. Subsequently, the samples were subjected to protease digestion by incubation with proteinase K and analyzed by SDS-PAGE followed by autoradiography.

However, incubation of the RNCs with the Sec61 complex resulted in protection of the full-length chain with different degrees of efficiency: most efficient was an excess of Sec61 complex in the detergent DeoxyBigCHAP (DBC), leading to about 75-85% protected chains. Higher concentrations of the Sec61 complex or the presence of phospholipids did not significantly change the degree of protection. In contrast, incubation with the Sec61 complex in Triton X-100 led only to 15-25% protected chains (Figure 3.11).

3.2.3 Reconstruction and Overall Structure of the RNC-Channel Complex

The RNC-channel complex reconstituted in DBC was used for structure determination by cryo-electron microscopy and single particle reconstruction. As a control, empty ribosomes were isolated from a translation system lacking mRNA and reconstituted under the same conditions with the Sec61 complex. Figure 3.12 shows the structures of the active and inactive complexes determined at a resolution of 15.4 Å and 18.9 Å, respectively, based on the Fourier shell correlation criterion using a cutoff at 0.5 (corresponding to 10.9 Å and 13.7 Å using a cutoff at 3*sigma). The lower resolution in the case of the non-translating ribosome is most likely a result of higher conformational variability due to a less defined functional state of the ribosome. The 15.4 Å (or 10.4 Å) reconstruction represents the highest resolution achieved so far for an eukaryotic 80S ribosome. It was further processed to separate rRNA from protein densities (Spahn et al., 2000) and interpreted by docking of rRNA and protein models (Spahn et al., 2001).

Both structures show the same overall appearance typical of the yeast 80S ribosome, with the small (40S) and large (60S) ribosomal subunits clearly recognizable (Figure 3.12) (Beckmann et al., 1997; Spahn et al., 2000; Gomez-Lorenzo et al., 2000, and Morgan et al., 2000). Extra density representing the Sec61 complex is visible in both reconstructions at the exit site of the large ribosomal subunit tunnel, which is believed to function as a conduit for the nascent chain (Bernabeu et al., 1983; Beckmann et al., 1997, and Nissen et al., 2000). The shape of the PCC in its active and inactive state is similar to the shape observed before (Beckmann et al., 1997) with a gap of at least 15 Å present between the channel surface and the ribosome, regardless of the presence of a signal sequence.

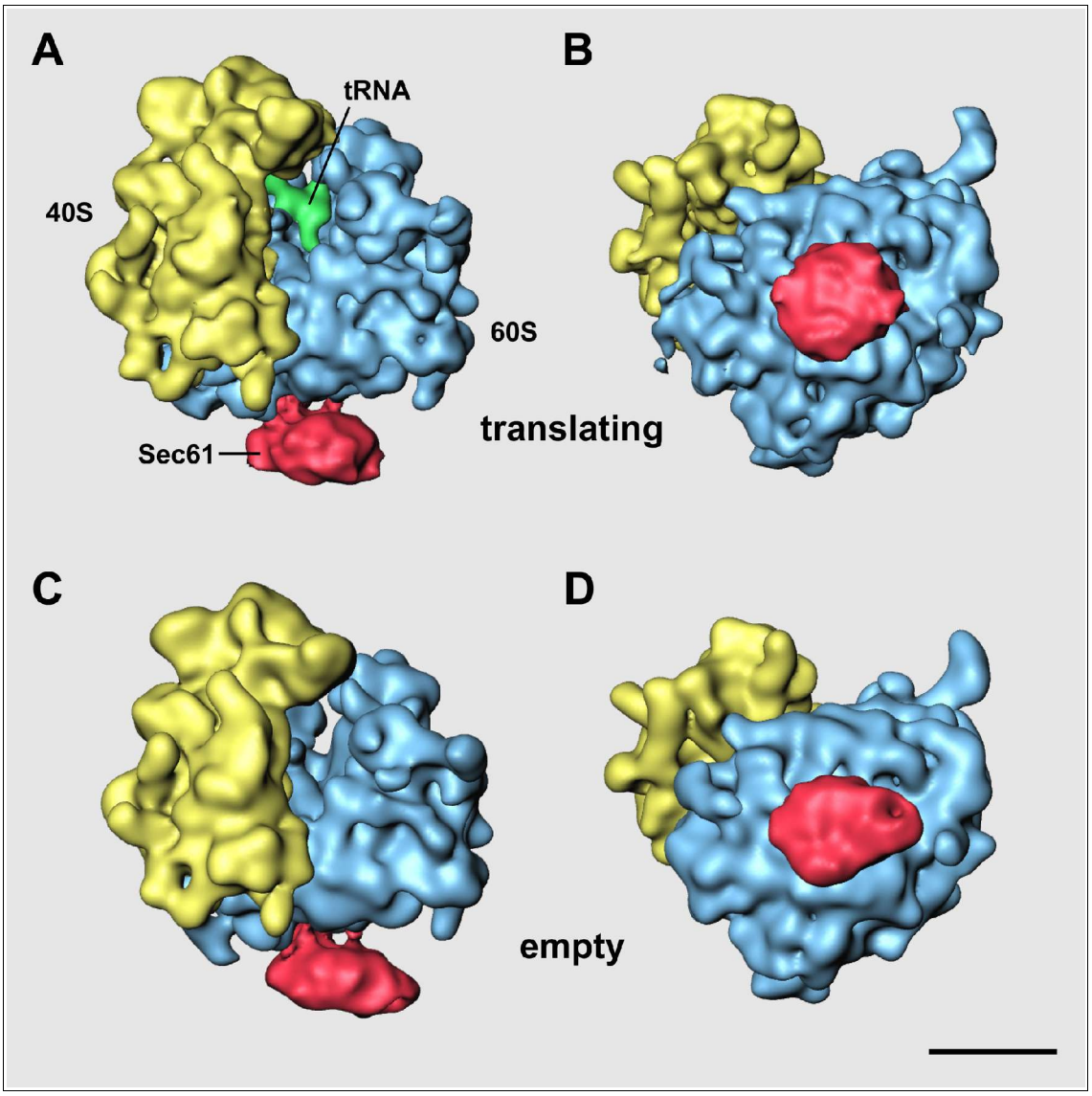

Figure 3.12: Cryo-EM structures of the translating and the empty ribosome-Sec61 complex. (A) Reconstruction of the translating and translocating RNC-Sec61 complex in DBC at 15.4 Å resolution. Note the presence of tRNA density in the P-site and the Sec 61 channel with the shape of a closed disk in the active complex. Color coding: yellow, small ribosomal subunit (40S); blue, large ribosomal subunit (60S); red, Sec61 complex; green, P-site tRNA. (B)Same as (A) but rotated upwards by 90 degrees. (C) Reconstruction of the empty complex in DBC at 18.9 Å resolution. Note the absence of tRNA density and the elongated shape of the channel. Color coding as described for (A). (D) Same as (C) but rotated upwards by 90 degrees. Bar = 100 Å.

However, in both states additional connections between the PCC and the ribosome are visible and, interestingly, the PCC now appears as a closed disk with a central indentation rather than a toroidal mass with a central pore. The inactive PCC is somewhat flattened in the direction perpendicular to the plane of the membrane and elongated in the plane of the membrane when compared to the active one. Furthermore, additional density is visible in the inter-subunit space of the programmed ribosome, unambiguously recognizable as tRNA.

3.2.4 Presence of tRNA in the Programmed Ribosome

The tRNA density is shown with the same contour level as the ribosome. It is located in the P site of the ribosome and corresponds to an occupancy of at least 80-90% of the ribosomes (Figure 3.12, see (Spahn et al., 2001) for further analysis). Difference maps using programmed and empty ribosome did not reveal any significant occupancy of the A site or E site with tRNA. tRNAs occupying A or E site were probably removed during the wash step using high salt concentrations. This result demonstrates that the translation of truncated mRNA indeed leads to a stalled peptidyl-tRNA with the vast majority tightly bound to the P site in a high-salt resistant manner. Furthermore, these results confirm the efficiency of the new protocol and the quality of the resulting preparation. The high occupancy of ribosomes with peptidyl-tRNA serves as proof for the presence of the signal sequence-containing nascent chain, which is small (~14 kDa) and too elongated to be visualized at this resolution. Similarly, visualization by cryo-EM of 70S ribosomes charged with tRNA *in vitro* (Agrawal et al., 1996; Agrawal et al., 2000) or of translating dimeric ribosomes formed *in vivo* (Stark et al., 1997b) also led to clearly identifiable tRNA densities in the inter-subunit space.

3.2.5 The Ribosome-Channel Connection

The connection between ribosome and channel is not circumferentially sealed but leaves a lateral opening of ~15 Å (Figure 3.12,3.13 and 3.14) in both reconstructions. This finding is similar to what has been observed at lower resolution in several ribosome-channel reconstructions from yeast as well as from mammalian complexes (Beckmann et al., 1997; Menetret et al., 2000). There is no significant difference in the dimensions of this gap when comparing active and inactive complexes (Figure 3.12,3.13). Even at very low contour levels, the ribosome-channel connection is never completely sealed regardless of the functional state (data not shown).

Docking of rRNA and protein models into separated rRNA and protein densities (Spahn et al., 2001) allowed the analysis of the PCC attachment sites on the molecular level (table 3.2). In both functional states the channel is attached to the ribosome with the same connections, one of which we observed before at lower resolution (connection 1, (Beckmann et al., 1997)). It is formed by a protrusion consisting of the helix 59 of rRNA domain III and the N-terminal domain of the ribosomal protein rpL19 (see table 3.2). However, three additional connections are now visible (Figure 3.13 and 3.14). Connection 2 most likely also involves rRNA domain III (helix 53 and helix 50) and the N-terminal domain of rpL19 as well as rpL25. Connection 3 is in closest proximity to the tunnel exit engaging rRNA helix 24 of domain I and, in addition, an extended loop of rpL26. Connection 4 is the most substantial one, involving two ribosomal proteins, rpL25 and rpL35, and the tip of rRNA helix 7 of domain I (Figure 3.13 and 3.14).

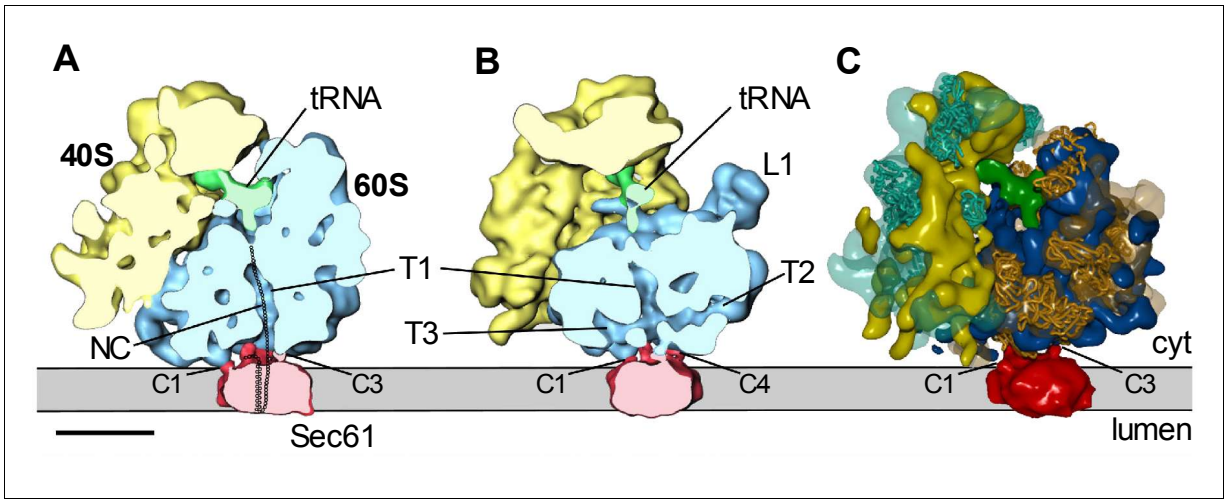

Figure 3.13: Connections, gaps and tunnels in the RNC-Sec61 structure. **(A)** The 15.4-Å reconstruction of the RNC-Sec61 complex as shown in Figure 3.12 but cut perpendicular to the plane of the membrane along the tunnel in the large ribosomal subunit. Color code as in Figure 3.12. C1 to C3 mark the connections between the ribosome and the channel. T1 marks the vertical tunnel, which functions as conduit for the nascent chain. The expected path of the nascent chain is indicated (NC). Note the gap between the ribosome and the channel. Cyt: cytosolic side, lumen: ER lumen. Bar = 100 Å. **(B)** As in (A) but rotated by 60 degree around the z-axis. T2 and T3 indicate the position of two horizontal tunnels connecting the main vertical (T1) with the cytosolic environment and C4 marks the fourth ribosome-channel connection. Note the gap between the ribosome and the channel. **(C)** Structure of the RNC-Sec61 complex after separating rRNA and protein densities, and docking of protein homology models into densities. Color code: red, Sec61 complex; green, P-site tRNA; blue, 25S/5S rRNA density; transparent orange, 60S protein density; orange, backbone of 60S protein models; yellow, 18S rRNA density; transparent turquoise, 40S protein density; turquoise, backbone of 40S protein models. Note the gap between the ribosome and the channel and the presence of rRNA as well as protein near the channel connections.

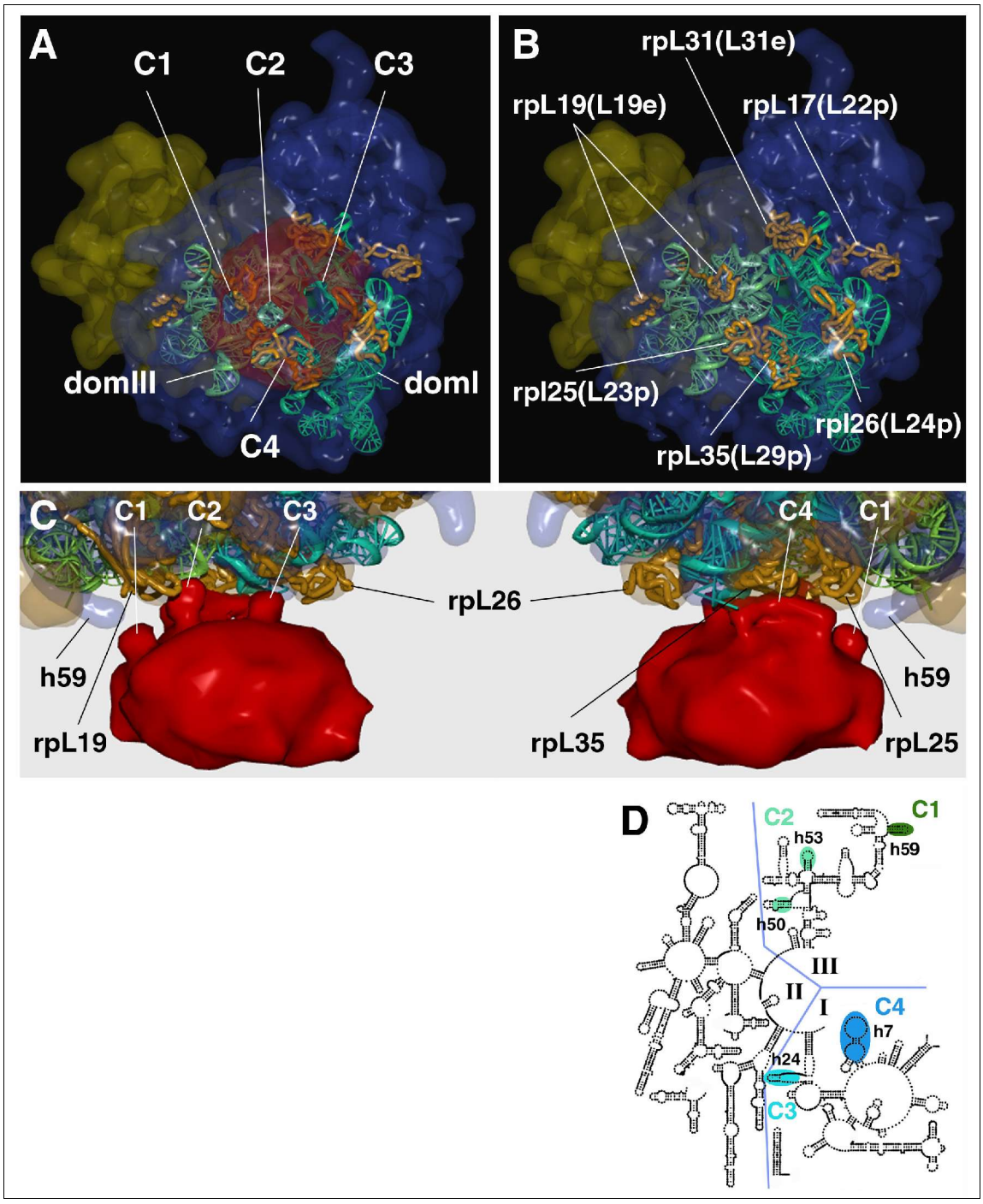

Figure 3.14: Molecular analysis the RNC-Sec61 connections. **(A)** The RNC-Sec61 complex is shown in the same orientation and color code as in Figure 3.12 B with transparent densities. Docked models of the 25S rRNA domains (turquoise, domI and domIII) involved in channel attachment and the backbones of homology models (orange) of the ribosomal proteins near the

tunnel exit are shown. The positions of the four connections (C1-C4) are indicated by holes in the Sec61 density. Note the particularly strong participation of ribosomal proteins in connection 4. **(B)** Same as in (A) but without the Sec61 density. Proteins are labeled according to yeast nomenclature with the corresponding ribosomal protein family name given in parenthesis. **(C)** Close up of the RNC-Sec61 junction in a similar orientation as in Figure 3.12 (left side) and rotated 180º around the z-axis (right side). The separated 25S rRNA and the 60S protein densities are shown in transparent blue and transparent orange, respectively. Docked models of the 25S rRNA domain I (turquoise), domain III (green) and proteins (orange) are shown as ribbons. The positions of the four connections (C1-C4) are indicated. Density for helix 59 of rRNA domain III is marked by h59. Participation in connection 1, rRNA domain III and rpL19 (L19e); connection 2, rRNA domain III and rpL19 (L19e); connection 3, rRNA domain I and rpL26 (L24p), connection 4, rRNA domain I, rpL25 (L23p) and rpL35 (L29p). For details see table 3.2. **(D)** Secondary structure diagram of the yeast 25S rRNA domains I, II and III. The regions involved in connection are labeled accordingly (for details see table 3.2).

Connection	***Protein***	***Position (yeast models)***	***25S rRNA***	***Position (archea model)***
1	rpL19 (L19e)	P25 – T48	helix 59 (dom III)	G1627-G1634
2	rpL19 (L19e)	P25 – T48	helix 53 (dom III)	G1498-C1507
	rpL25 (L23p)	S68 – I80	helix 50 (dom III)	C1421-A1424
3	rpL26 (L24p)	T86-P96	helix 24 (dom I)	G504-G487
4	rpL25 (L23p)	S68-I80, A127-A135	helix 7 (dom I)	G81-G94
	rpL35 (L29p)	A2-K5, K25-K49		

Table 3.2: Molecular analysis of the ribosome-channel connections

3.2.6 Structure and Function of the Protein-Conducting Channel

The dimensions of the PCC are similar to findings of earlier EM studies (Hanein et al., 1996; Beckmann et al., 1997 and Menetret et al., 2000). The distance between cytosolic and lumenal surface measures about 45 Å, easily spanning the membrane. The diameter of the translocating channel is between 90-100 Å (Figure 3.14). The channel associated with the empty ribosome appears slightly flattened and elongated towards the backside of the large ribosomal subunit with a diameter of 105 Å. This elongation is lost at higher contour levels, where translocating and non-translocating channels appear more similar (data not shown). Although the channel density displays structural details, the slightly pentagonal shape that was described in previous studies of the Sec61 complex (Hanein et al., 1996; Beckmann et al., 1997) and in one study of its bacterial homologue, the SecYE complex (Meyer et al., 1999), is not recognizable. Remarkably, in both functional states the channel appears compact and show only a small indentation instead of a central pore (Figure 3.15 A)

For an estimation of the Sec61 oligomer stoichiometry, we used the channel density in the following way: each Sec61 trimer is believed to have 12 membrane-spanning helices plus two amphipatic helices (Wilkinson et al., 1996; reviewed in Johnson and van Waes, 1999). Assuming membrane-specific helix packing, we determined the number of helices of known membrane protein structures that could fit into the channel density. This approach is reliable even in the presence of flexible and thereby invisible domains outside the membrane, in contrast to calculations based on observed volume and specific protein density. Assuming less dense packing in the central region, the channel density offers space for 35 helices (i.e. provided by five rhodopsin molecules, Figure 3.15 B,C).

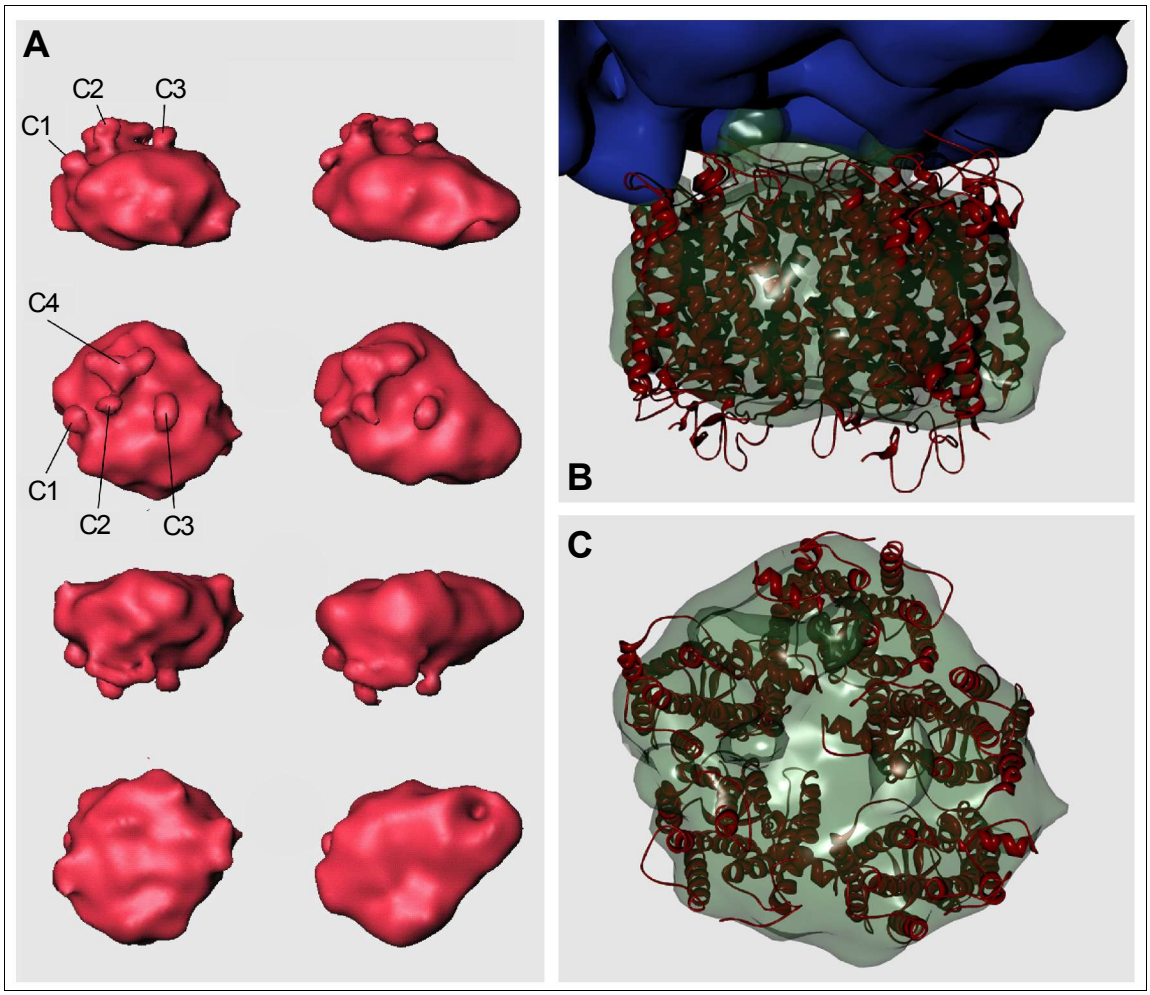

Figure 3.15: Structure and stoichiometry of the protein-conducting channel. **(A)** Isolated density of the Sec61 complex in the translocating state (left column) and the inactive state (right column). The view on top is the same as in Figure 3.12 A and C. The views below are rotated 90, 180 and 270º towards the viewer. The four connections are marked by C1 to C4. Note the central indentation at the surface facing the ER lumen and the ribosome. The channel attached to the empty ribosome appears elongated and flattened compared to the one engaged in translocation. **(B)** Close-up of the RNC-Sec61 junction in the same orientation as in (A) with the large ribosomal subunit shown in blue and the Sec61 complex in transparent green. In order to estimate the stoichiometry of the Sec61 oligomer, the transmembrane helices of five rhodopsin molecules (red ribbons) were fitted into the channel density. **(C)** Top view of (B), but only the channel density with fitted membrane domains. The number of approximately 35 helices fitting into the density suggests a trimer of Sec61 trimers (36 helices).

3.3 The GTPase Cycle of the SRP Receptor β-Subunit

3.3.1 Sbh1p and Sbh2p share Sequence Homology with the Sec7 domain

GEFs for several families of GTPases have been functionally and structurally characterized. Interestingly, GEFs vary dramatically in structure. However, those specific for one family of GTPases usually have the same fold. Accordingly, the GEFs for the GTPases of the ARF-family share a common functional region of about 200 amino acids, the Sec7 domain (reviewed in Jackson and Casanova, 2000).

Taking the structural similarity between SRβ and ARF into account, a similarity between the respective GEFs is also conceivable. Searching the sequence database, we could identify significant sequence similarity between the cytosolic domains of the two subunits of the PCCs in yeast (Sbh1p and Sbh2p) and the Sec7 domains of several GEFs for GTPases of the ARF-family from yeast (Figure 3.16).

The sequence similarity involves the regions of Sec7 that is crucial for GEF function, namely the F-G loop and helix H (Goldberg et al., 1998). Based on these findings, we tested whether Sbh1p and Sbh2p are able to promote the exchange of nucleotide for SRβ.

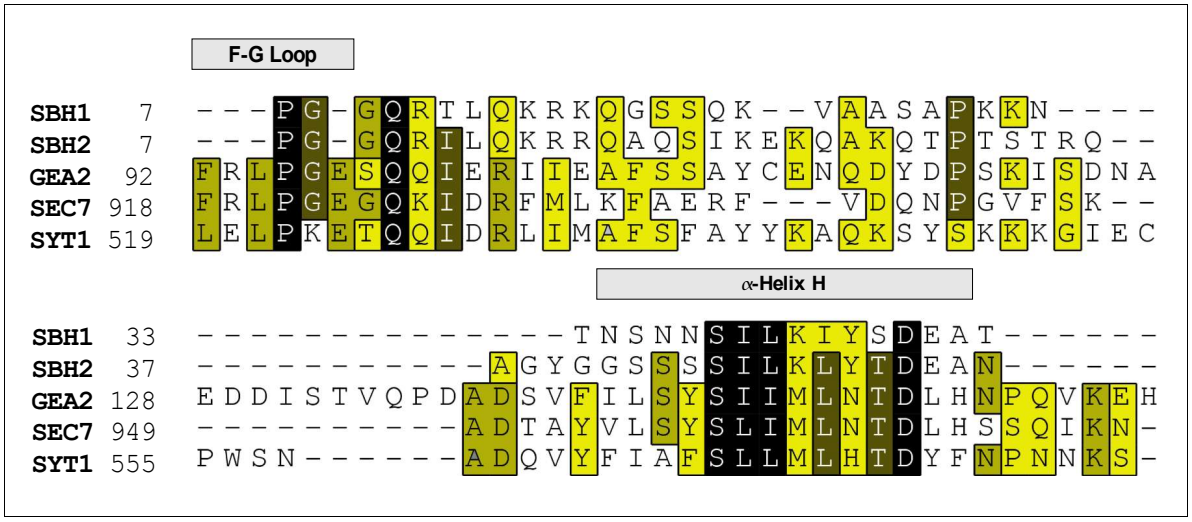

Figure 3.16: Sequence comparison between Sbh1p/Sbh2p and the Sec7 domain. Sequence alignment of Sbh1p and Sbh2p with the Sec7 domains of the ARF GEFs Gea2p, Sec7p and Syt1p from yeast. Sequences are coded using a gradient from yellow to black indicating increasing sequence similarity. Numbers indicate the residues of the proteins except in the case of Gea2p where the numbering adheres to the published numbering scheme of the Sec7 domain (Goldberg et al., 1998).

3.3.2 Sbh1p and Sbh2p function as the GEFs for SRβ

A fluorescence spectroscopic assay was used, which allows one to monitor the nucleotide exchange on a G-protein in real-time and at high resolution. It had been shown that the fluorescent signal of 3'-(N-Methyl-anthraniloyl)-2'-deoxy-guanosine-5'-diphosphate (mantGDP) is dependent on the environment of the probe and hence on the amount of mantGDP bound by a G-protein (Lenzen et al., 1995). Recombinant yeast SRβ31-244 was purified from *E. coli* and endogenously bound nucleotide removed by size exclusion chromatography in the presence of EDTA (Figure 3.17).

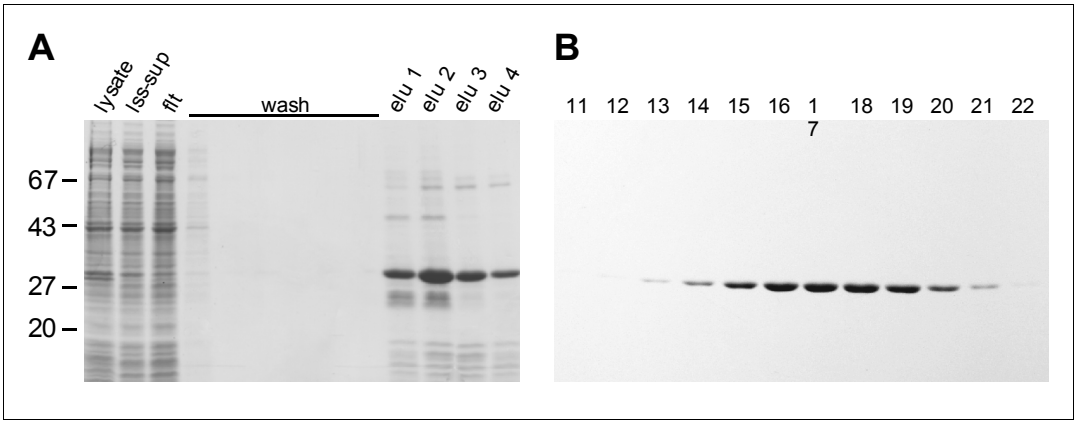

Figure 3.17: Purification of SRβ31-244. **(A)** SRβ31-244 was purified by metal affinity chromatography by clearing a cell lysate (lys) by low-speed centrifugation (Flss-sup) and incubating the supernatant with TALON™ metal affinity resin (flt shows unbound protein). The resin was washed 3x times with lysate buffer and 4x times with lysate buffer containing 400 mM NaCl (wash). Protein was eluted using 200 mM imidazole in lysate buffer (elu1-elu4). Aliquots of fractions were separated by SDS-PAGE and stained with Safe-Stain.
(B) The pooled elution fractions from (A) were subjected to size exclusion chromatography using a Superdex-75 column. Fraction aliquots of a single A_{280} peak of SRβ31-244 were separated by SDS-PAGE and stained with safe-stain. Fractions 16-19 were pooled and stored at -80ºC.

The removal of nucleotide from SRβ31-244 was confirmed by HPLC analysis and determined to be complete (Figure 3.18).

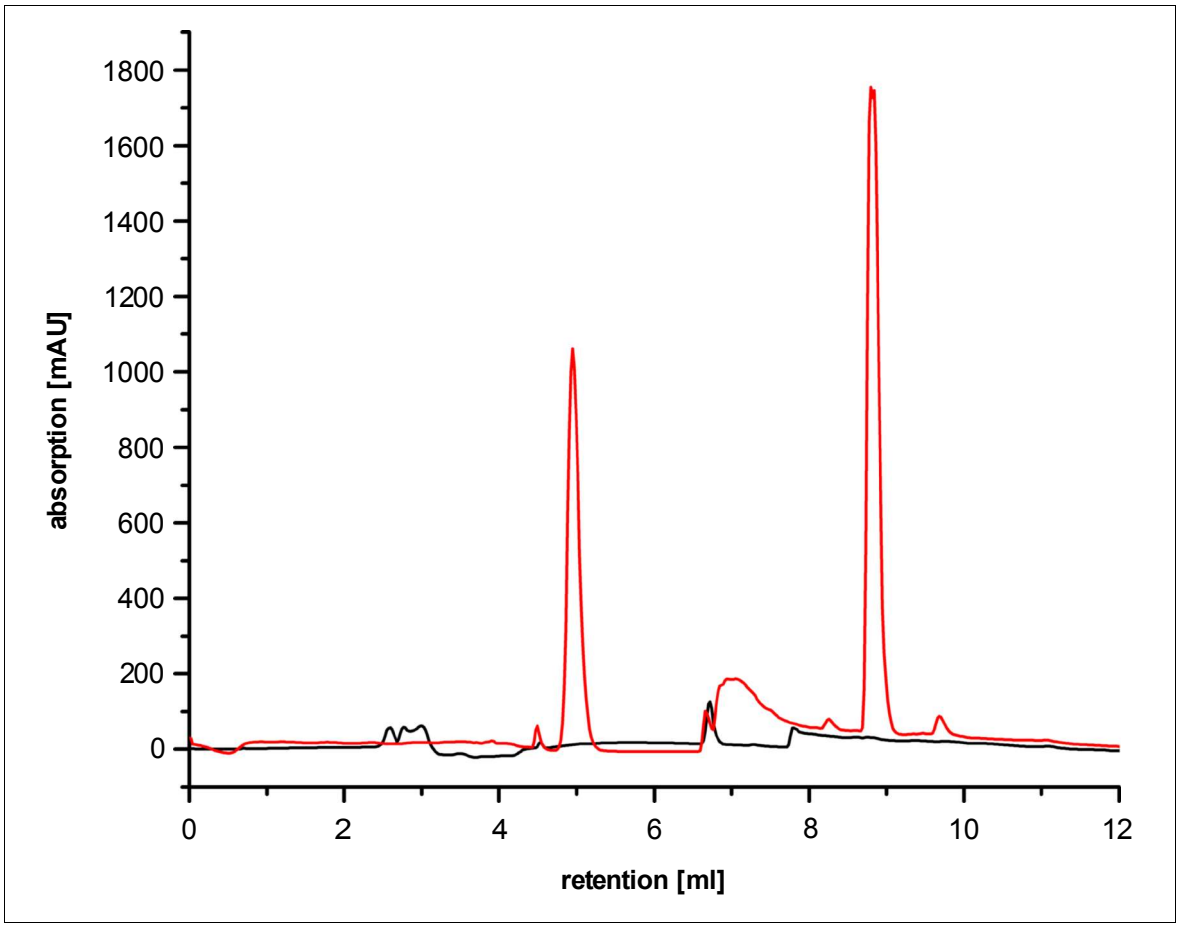

Figure 3.18: HPLC analysis of nucleotide free SRβ31-244. The removal of endogenous nucleotide from SRβ31-244 was confirmed by HPLC analysis: 500 µl of 30 µM GDP and mantGDP (red line) or 30 µM denatured SRβ31-244 (black line) in buffer A [100mM TEA (pH 8.0) and 10 mM tetra-butyl-ammonium-sulfamat] were separated on a C18-column using a 0-100% gradient of buffer A to buffer B [100mM TEA (pH 8.0), 10 mM tetra-butyl-ammonium-sulfamat and 50% acetonitril].

SRβ31-244 was reloaded with nucleotide by incubation with an excess of mantGDP and unincorporated mantGDP was removed by dialysis. The reloading of SRβ31-244 with mantGDP resulted in a substantial increase of emitted fluorescence compared to mantGDP alone (Figure 3.19). The SRβ31-244 dependent increase averaged 20%, indicating that mantGDP was successfully bound by SRβ31-244.

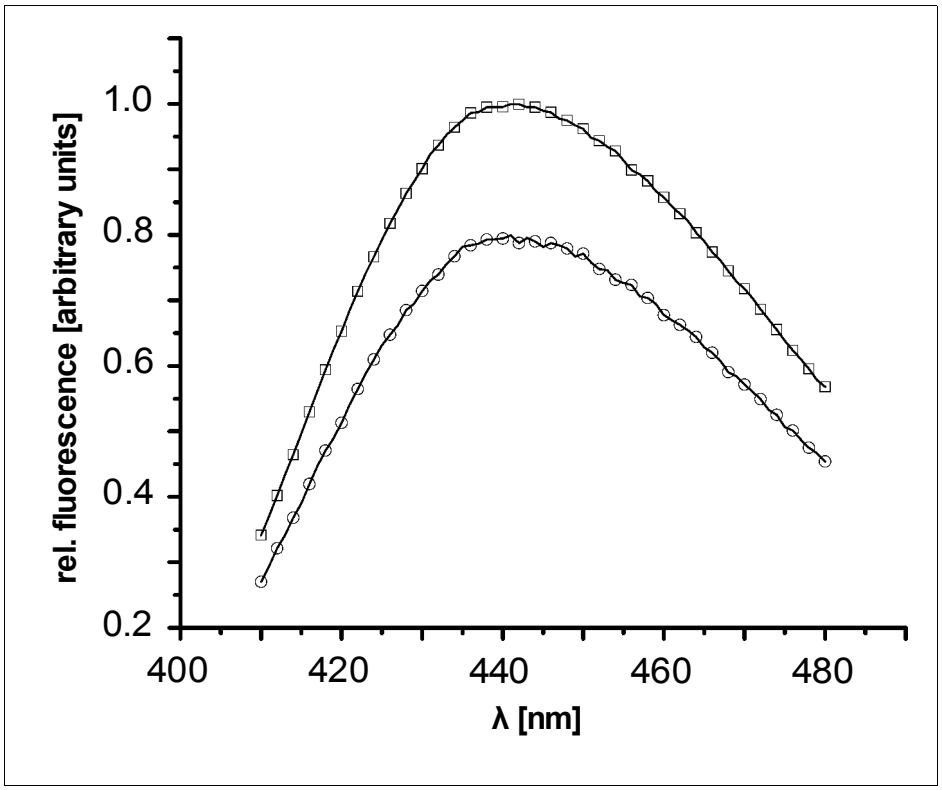

Figure 3.19: Fluorescence enhancement on binding mantGDP to SRβ31-244. 10 µM mantGDP (○) or 10 µM of mantGDP-SRβ31-244 (□) were excited at 352nm and emission was recorded between 410 and 480 nm at 25 ºC. SRβ31-244 did not emit in the range of wavelengths recorded.

The *SBH1* gene in yeast codes for a 8.7 kDa protein with a COOH-terminal transmembrane domain. Its homologue Sbh2p is slightly larger with a size of 9.6 kDa. To test whether Sbh1p or Sbh2p are directly involved in the nucleotide exchange of SRβ, we purified the recombinant N-terminal cytosolic domains of Sbh1p (Sbh1pΔC) and Sbh2p (Sbh2pΔC) by GST affinity chromatography (Figure 3.20).

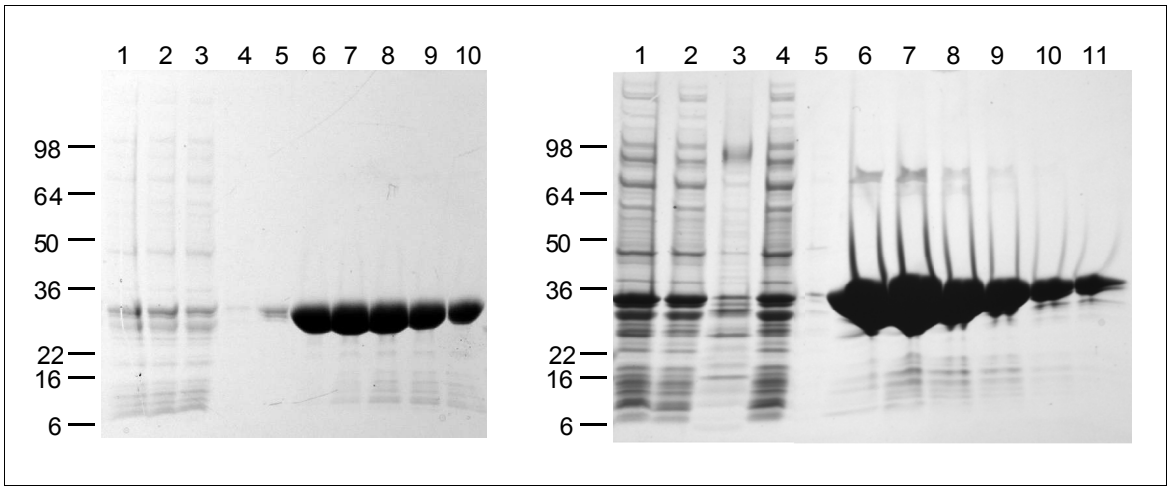

Figure 3.20: Purification of recombinant GST-Sbh1pΔC and GST-Sbh2pΔC. The GST-tagged proteins were purified from cleared cell lysates by GST affinity chromatography. **(A)** Purification of Sbh1pΔC: lane 1, lysate; lane 2, low speed supernatant; lane3, unbound protein; lane 4, wash; lanes 5-10 elution fractions. **(B)** Purification of GST-Sbh2pΔC: lane 1, lysate; lane2, low speed spin supernatant; lane 3 low speed spin pellet; lane4, unbound protein; lane 5, wash; lane 6-11, elution fractions. Molecular weights are indicated in kDa.

Equimolar amounts of mantGDP-SRβ31-244, GST-Sbh1pΔC, or GST-Sbh2pΔC in the presence of an excess of GDP were incubated at 25 ºC. The reactions were excited at 352nm and the emission recorded at 441 nm. When incubating mock buffer with mantGDP-SRβ31-244, no decrease of fluorescence could be detected (Figure 3.21, panel A). This result indicates that SRβ31-244 binds nucleotide tightly and does not exchange with the solution by itself. When using GST alone in the assay, no decrease in fluorescence could be detected either (Figure 3.23).

In the presence of GST-Sbh1pΔC or GST-Sbh2pΔC, a substantial decrease of fluorescence could be measured resulting from the exchange of nucleotide. The observed decrease of fluorescence averaged 12% after 15 minutes (Figure 3.21, panel A) and reached a plateau after a decrease of 14% (data not shown).

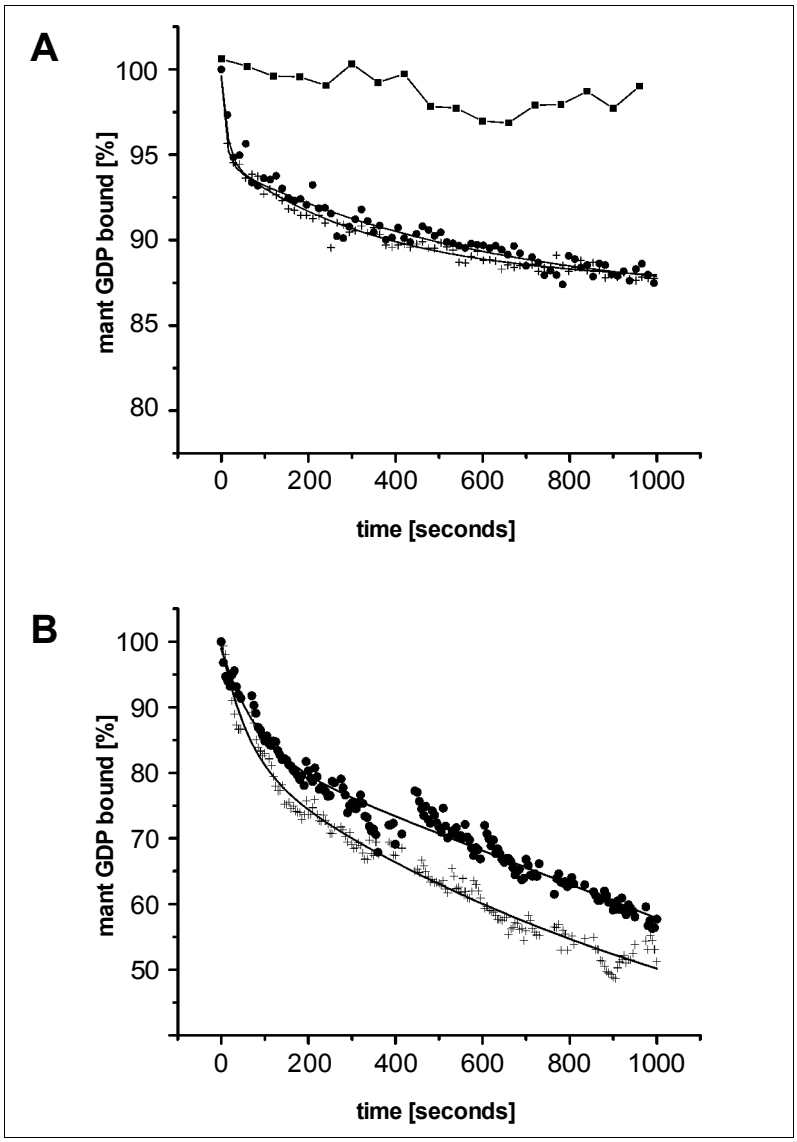

Figure 3.21: Dissociation of mantGDP from SRβ31-244. **(A)** Comparison of the intrinsic (■) and Sbh1p (●) or Sbh2p (+) stimulated dissociation of mantGDP from SRβ31-244. 1 µM mant-SRβ31-244 was incubated with either mock buffer or 1 µM GST-Sbh1pΔC or GST-Sbh2pΔC at 25 ºC in the presence of GDP (100 µM). The data was fitted as the sum of two exponentials resulting in the following rate constants: Sbh1p: k_1=9.4x10^{-2}, k_2=2.3x10^{-3}; Sbh2p: k_1=13.9x10^{-2}, k_2=3.7x10^{-3}. **(B)** 1 µM mant- SRβ31-244 was incubated with 10 µM GST-Sbh1pΔC (●) or GST-Sbh2pΔC (+) at 25 ºC in the presence of GDP (100 µM).

The obtained data were best fitted as a sum of two exponential decays. When a ten fold excess of either GST-Sbh1pΔC or GST-Sbh2pΔC over SRβ31-244 was used in the assay, the decrease of fluorescence averaged 50%, indicating that GST-Sbh1pΔC and GST-Sbh2pΔC do exchange the nucleotide of SRβ stoichiometrically rather than catalytically (Figure 3.21 B).

3.3.3 Sbh1p functions as the GEF for SRβ in the Trimeric Sec61p but not in the Heptameric Complex

Sbh1p is assembled into two different PCCs in yeast. It is not only part of the trimeric Sec61p complex involved in cotranslational protein transport, but also part of the heptameric complex that is exclusively involved in posttranslational protein transport. To test whether the GEF activity for SRβ is dependent on the assembly state of Sbh1p, we purified the trimeric Sec61p- and the heptameric complex from yeast and tested both detergent-solubilized complexes in the nucleotide exchange assay.

We incubated equimolar amounts of mantGDP-SRβ31-244 with trimeric Sec61p complex or heptameric complex in the presence of an excess of GDP at 25 ºC. When mantGDP-SRβ31-244 was incubated with purified trimeric Sec61p complex, mantGDP was efficiently exchanged with GDP, resulting in a decrease of fluorescence that averaged to 17% after 15 minutes (Figure 3.22) and reached a plateau after a decrease of 20% (data not shown).

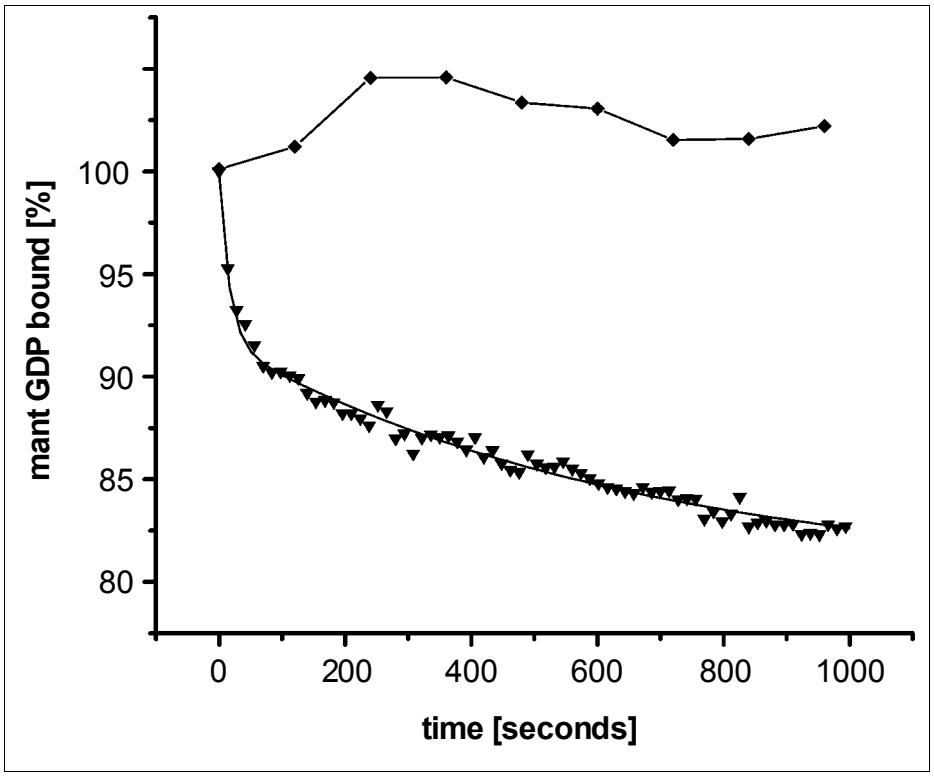

Figure 3.22: Comparison of the effect of trimeric Sec61p complex (▼) or heptameric complex (◆) on the dissociation of mantGDP from SRβ31-244. 1 µM mant-SRβ31-244 was incubated with either 1 µM trimeric Sec61p complex or heptameric complex at 25 ºC in the presence of GDP (100 µM). The data was fitted as the sum of two exponentials resulting in the following rate constants for the Sec61p complex: $k_1=8.4x10^{-2}$, $k_2=2.1x10^{-3}$.

The obtained data was best fitted as a sum of two exponential decays. When using equimolar amounts of mantGDP-SRβ31-244 and purified heptameric complex, no decrease in fluorescence could be detected (Figure 3.22), indicating that Sbh1p is not able to function as the GEF for SRβ when assembled into the heptameric complex.

The ribosome had been reported to reduce the affinity of SRβ for nucleotide (Bacher et al., 1999), and therefore was proposed to function as the GEF for SRβ (Fulga et al., 2001). To test whether the ribosome is able to promote the exchange of nucleotide for SRβ, we used purified translating and non-translating ribosomes in the GTPase exchange assay. In our system, neither translating nor non-translating ribosomes were able to exchange the nucleotide of SRβ (Figure 3.23).

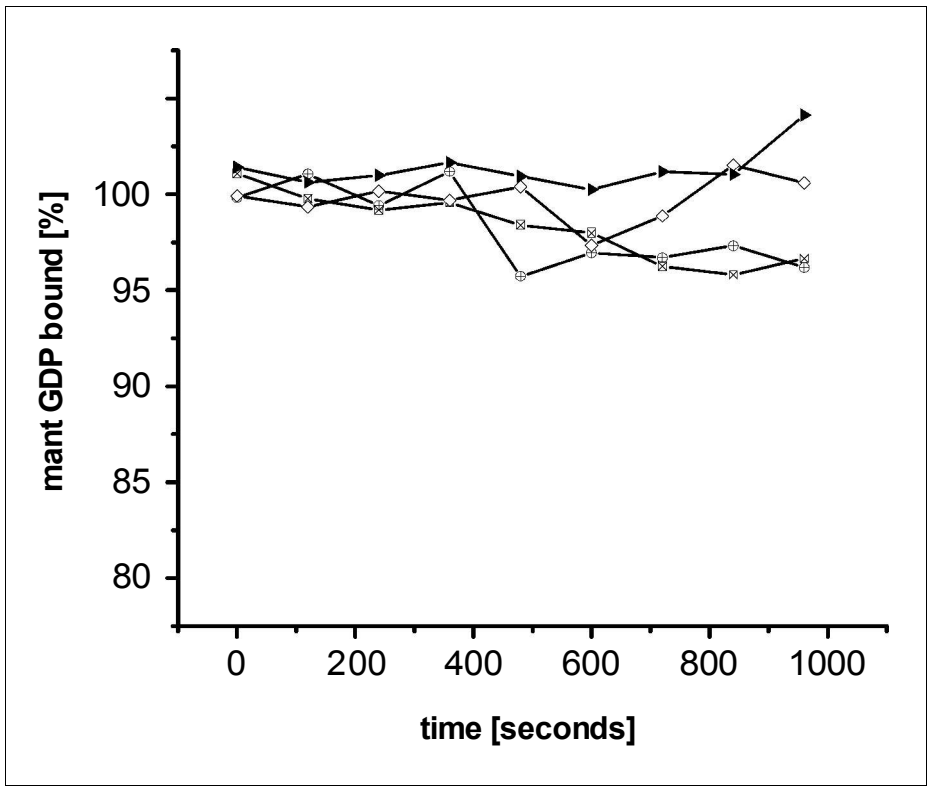

Figure 3.23: Comparison of the effect of non-translating ribosomes (⊠), translating ribosomes (⊕), GST (▶) or the SRP (◇) on the dissociation of mantGDP from SRβ31-244. 1 µM mant-SRβ31-244 was incubated with either 1 µM non translating ribosomes, GST, SRP or 1nM translating ribosomes at 25 ºC in the presence of GDP (100 µM).

To exclude the possibility that other components of the co-translational targeting pathway might have an influence on the exchange of nucleotide for SRβ, we tested whether the SRP is able to promote the exchange of nucleotide for SRβ. When using purified SRP from yeast in our nucleotide exchange assay, the SRP was not able to exchange the nucleotide for SRβ (Figure 3.23).

We conclude that Sbh1p and Sbh2p are the GEFs for SRβ. Both proteins are able to efficiently promote the exchange of nucleotide for SRβ. The nucleotide exchange activity of Sbh1p is not dependent on the other subunits of the trimeric Sec61p complex. Furthermore, Sbh1p is able to promote the nucleotide exchange for SRβ when assembled into the trimeric Sec61p complex but not when assembled into the heptameric complex.